Libyan Journal of Applied and Contemporary Sciences
ISSN
E: 3136-3709
L: 3136-3695
Vol 1: No 2

A Physics-Informed Neural Network Based on the Separation of Variables for Solving a Distributed-Order Dispersive Generalized Hunter–Saxton Model with Fractional-Time Effects

Zena Talal Yassin[1*]

[1] Department of Mathematics, College of Computer Science and Mathematics, University of Mosul, Mosul, Iraq

Email corresponding author's: zena-talal@uomosul.edu.iq

Received: 1/7/2026 Accepted: 15/8/2026 Published: 2/9/2026

Copyright © 2026 Author(s) ; Published by Libyan Journal of Applied and Contemporary Sciences
This is an open access article licensed under CC BY: (https://creativecommons.org/licenses/by/4.0)

Abstract

This paper presents and examines an extension of the generalized Hunter-Saxton equation to higher order of dispersion. The model in its classical form is defined as, $\Upsilon_{tx} = \Upsilon\Upsilon_{xx} + \beta\Upsilon_x^2 + \varepsilon\Upsilon_{xxxx}, 0 < \varepsilon < 1$. Where the dispersive/regularizing high-order term added to the model adds to the traveling-wave dynamics over the non-dispersive case. We measure the effects of the fractional-time by looking at time-fractional analogs of three standard operators the modified Riemann Liouville derivative, the -type derivative and the M-truncated derivative and show that the fractionalization changes the effective traveling-wave variable and introduces observable changes in the localization and propagation of waves. In order to unify retention of nonlocal memory effects, we also propose a distributed-order time-fractional correction where the time operator operates on the slope field Υ_x, $D_t^{\omega(\alpha)}(\Upsilon_x) = \Upsilon\Upsilon_{xx} + \beta\Upsilon_x^2 + \varepsilon\Upsilon_{xxxx}$, Because Caputo-type distributed-order operators contain history integrals that cannot be directly addressed using standard automatic differentiation, we introduce a separation-of-variables physics-informed neural network (SVPINN) model that parametrizes the distributed-order correction by a trainable surrogate model. Lastly, numerical diagnostics of the related reduced dynamical system display high sensitivity to initial perturbations, limited transverse oscillations in some regimes, a non-isolated equilibrium manifold that causes switching between neutral drift, center-type oscillations, and saddle-type behavior. On the whole, it can be concluded that fourth-order dispersion and fractional-time processes and, to a great extent, distributed-order memory significantly add to the qualitative dynamics of Hunter Saxton-type model.

Keyword: Dispersive Hunter-Saxton equation; Traveling waves; solitons; SVPINN; physics-informed neural networks; Sensitivity and stability analysis.

Doi : https://doi.org/10.64943/ljacs.2026.010208

INTRODUCTION

The Hunter Saxton (HS) equation holds a pivotal place in the analysis of the nonlinear wave propagation, especially in nonhomogeneous continuous media. It occurs as a natural consequence in the modelling of the orientational dynamics of nematic liquid crystals, in which it models the dynamics of the director field under the combined influence of elastic deformation and inertia [1]. In addition to its physical applicability, the HS equation has been of particular interest because of its unique analytical and geometrical form. Specifically, it has a geometric interpretation as a geodesic flow on the right-invariant Sobolev metrics of suitable configuration spaces, and it has very strong nonlinear behaviors, such as finite-time gradient blow-up, and the appearance of cusp-like singularities [3,4]. Bressan and Constantin [5] formulated a basic well-posedness theory and built global conservative and dissipative weak solutions based on the tools of optimal transport. Additional properties of stability and unicity can be interpreted in the larger generalized Proudman-Johnson system where the HS equation is a special case [6].

The generalized HS equation is a natural extension of the classical theory, with the nonlinear structure of transport maintained, but allowing a more flexible set of dynamical behaviors. Another characteristic of this generalized model that is of special significance is the richness of it in terms of integrability. The existence of a Lax representation and local and nonlocal recursion operators were defined by Morozov [7], which proved the full integrability. His previous research also demonstrated that the generalized HS equation is tangentially the same as a special Euler Poisson equation and obtained its general solution by using differential-geometric symmetry techniques [8]. Regardless of such progress, recent research has indicated that the generalized HS model continues to only admit a restricted category of traveling-wave solutions and the classical model does not possess strong enough higher-order dispersive processes to produce actually propagating wave profiles [9]. Such structural constraint drives the construction of dispersive extensions that can add the related wave dynamics.

We suggest and discuss a fourth-order dispersion extension of the generalized Hunter-Saxton model by adding a higher-order spatial dispersion term and to capture the effects of multi-scale memories, we substitute the classical time time-derivative of the slope field by a distributed-order Caputo time-derivative. In particular, we take into account the distributed-order dispersive Hunter Saxton formulation [9]:

$$D_t^{\omega(\alpha)}(\Upsilon_x) = \Upsilon\Upsilon_{xx} + \beta(\Upsilon_x)^2 + \varepsilon\Upsilon_{xxxx}\,, \varepsilon \ll 1, \tag{1}$$

Where the distributed-order operator is defined by

$$D_t^{\omega(\alpha)} q(x,t) = \int_0^1 \omega(\alpha)\, {}_0^C D_t^{\alpha} q(x,t) d\alpha \tag{2}$$

with $\omega(\alpha) > 0$ and $\int_0^1 \omega(\alpha) d\alpha < \infty$. This is a natural choice since the initial equation can be expressed as an evolution equation of $u = \Upsilon_x$, and an operator which is a distributed order can simply be extended to u_t to produce a multi-scale memory operator. The single parameter β is important in the determination of the qualitative dynamics of the emerging traveling-wave characteristics. The addition of the fourth-order dispersive term essentially changes the analytical form of the governing equation, thus allowing truly propagating traveling-wave profiles that are not allowed by the classical (non-dispersive) model. In addition, when ε is small, either in the vanishing-dispersion limit ε→0, the extended equation smoothly reduces to the standard generalized Hunter Saxton equation, and the related families of solutions degenerate to the already known stationary traveling-wave branch. This restrictive act proves the consistency of analytical scheme of the suggested dispersive extension.

To clarify the terminology associated with the fourth-order spatial term, we consider the linearized local dispersive core of the model. Let

$$u(x,t) = u_0 + \eta(x,t), |\eta| \ll 1,$$

where u_0 is a constant background state. Neglecting all terms that are quadratic or higher order in η, the nonlinear Hunter-Saxton terms reduce to their linear contribution, while the fourth-order spatial term remains explicitly present. We then introduce the Fourier normal-mode ansatz

$$\eta(x,t) = \hat{\eta} e^{i(kx-\omega t)}.$$

Consequently,

$$\partial_x^n \eta = (ik)^n \eta, \partial_t \eta = -i\omega\eta,$$

and the linearized governing equation yields a spectral relation of the general form

$$\mathcal{D}(\omega, k; u_0, \varepsilon) = 0,$$

The specific physical interpretation of the fourth-order spatial contributions depends on how it (the k^4 term) evolves in time. If the new frequency $\omega = \omega(k)$ which is a function of wave-number k^4, is real, and dependent non-linearly upon k, then each Fourier mode will have a different phase velocity.

$$c_{\mathrm{p}}(k) = \frac{\omega(k)}{k},$$

and the corresponding effect is dispersive. In contrast, if $\omega(k)$ possesses a nonzero imaginary component,

$$\mathrm{Im}(\omega(k)) \neq 0,$$

the amplitude of the perturbation will be exponentially increased or decreased. In this regard, fourth-order contributions are related to either linear instability or stabilizing (dissipating) / regularizing behavior and not purely dispersive. For that reason, through-out the paper the term "dispersive" is used only when supported by the appropriate linearized spectral relationship. In cases in which the specific mechanism responsible for the dynamics cannot be identified based upon the differential order of the spatial terms, we prefer the use of the term "fourth-order dispersive/stabilizing term," since the dynamic function of a fourth-derivative operator can depend on whether the operator is positive or negative; if placed in an equation as part of the spatial derivative versus time-evolution; or how the operator functions within the entire problem.

Fourth-order spatial derivatives arise in curvature- and surface-tension-driven models. In thin-film dynamics, Υ_{xxxx}, stabilizes the free surface and regularizes short-wavelength perturbations [10]. Fourth-order operators are also used in structural mechanics and beam theory, where they model bending resistance, and the transverse response of beams and plates to applied loads [11]. Similar fourth-order terms can also be found in phase separation, surface-tension-driven transport and pattern formation models, where they are usually understood to produce gradient flows which are related to curvature-dependent energies [12]. One such example is the Kuramoto Sivashinsky equation [13], where the destabilizing second-order diffusion is counterbalanced by stabilizing fourth-order dissipation to generate complex, but bounded spatiotemporal dynamics. Taken together, these arguments give a definite physical and analytical explanation of the need to implement the fourth-order dispersive term Υ_{xxxx}, into the generalized Hunter-Saxton model.

In science and engineering, modeling and solution of complicated physical systems in an efficient way are still crucial issues. Classical numerical methods, like finite element and finite difference methods, may have practical constraints when used to large-dimensional problems or domains with complex geometry and boundaries where computational cost may rapidly increase, and repetitive solves are needed to study parameters, to solve an inverse problem, or to estimate uncertainty. Physics-inspired neural networks (PINNs) [10] have been inspired by recent developments in machine learning, especially the high-capacity function approximation based on deep learning, and put governing equations and physical constraints directly into the objective of the training process, providing an alternative data-efficient simulation and inference paradigm.

PINNs have since been quite successful in a broad application to fluid mechanics [11,12,13,14], solid mechanics [15,16,17], heat conduction [9,10], and materials science [18]. Many improvements have been suggested to enhance accuracy, robustness and convergence. In the modeling front, these are network architecture modifications [12,13,14,15,16], integration of the attention mechanisms [17] and adaptive learning methods [18], better loss constructions and balancing schemes [19,20,21,22], and optimized training strategies and protocols [23,24,25]. Problem-structure Problems can be better captured by methods like domain decomposition [26,27], by the addition of more physics-based constraints [28,29,30], to improve localized features, reduce spectral bias and improve overall generalization and computational efficiency.

We also propose a physics-informed learning model (separation-of-variables PINN) to solve the distributed-order, dispersive extension of the generalized Hunter Saxton model to analyze the equations in a form beyond closed-form traveling-wave reductions. The point is that the distributed-order Caputo operator can be redefined as a surrogate of the kernel based on a variable separation, which will allow the distributed-order derivative to be computed directly as a part of the neural-network training cycle, instead of relying on a fixed numerical discretization of the underlying history integral. This offers a data-driven pathway to the proposed nonlocal-in-time model that conserves the physics governing it with residual-based constraints.

Stability and sensitivity properties are often the determining factors of the qualitative behavior of nonlinear evolution equations particularly when the equation is high-order in space, and high-order in time (high-order in time, high-order in space). Basic equilibrium stability, invariant bifurcation, Lyapunov and sensitivity with respect to initial data and parameters are systematically developed in the classical book of Khalil [22]. Wiggins [23], Strogatz [24], and Az-Zo'bi et al., [25,26] introduce complementary geometric and topological perspectives on the dynamics of phase-space bifurcations and chaotic attractors. The deterministic chaos and global dynamical structures have been thoroughly treated by Cvitanovic et al. [27].

The current analysis is based on the SVPINN equation approach presented in [28], which offers a single analytical approach incorporating classical reductions, such as Riccati-, Bernoulli-, and linear-type auxiliary equations. Through a traveling-wave transformation, the proposed dispersive Hunter Saxton model can be simplified into a nonlinear ordinary differential equation (NODE) and new families of exact single-wave solutions can be built. These solution classes consist of trigonometric, hyperbolic, exponential and similar closed-form structures, which occur under certain parameter regimes (that is, when certain values of 0 are selected). In addition, driven by the increased importance of a fractional calculus as a model of memory and hereditary effects in complex media [29,30,31,32,33], we solve the model in time-fractional contexts, where the classical time derivative is replaced by the modified Riemann Liouville, beta and M truncated derivatives, and monitor the resulting modifications using the corresponding traveling-wave reductions. Lastly, we supplement the exact-solution analysis with a qualitative exploration of the reduced NODE, pointing out the most significant dynamical effects of the dispersive extension of the equation of state to be proposed, namely, Eq (1). The principal contributions of this work are as summarized as follows:

- We introduce a fourth-order dispersive generalization of our generalized Hunter Saxton model, and derive its distributed-order time-fractional form by replacing $u = \Upsilon_x$, yielding $D_t^{\omega(\alpha)}(\Upsilon_x) = \Upsilon\Upsilon_{xx} + \beta(\Upsilon_x)^2 + \varepsilon\Upsilon_{xxxx}$ with $0 < \varepsilon \ll 1$.
- We explore effects of time fractionality with three typical time fractional operators (modified Riemann-Liouville β -type, and M-truncated derivatives) and show that the effective traveling-wave variable is altered by fractionalization, resulting in operator-dependent changes in wave localization and propagation.
- We come up with a formulation of SVPINN on the distributed-order model that does not prescribe a fixed discretization of Caputo-type history integrals by using auxiliary network outputs and a separable surrogate representation of the distributed-order term, and an extra physics-based consistency constraint.
- We give quantitative information and diagnostics, such as SVPINN benchmark tests with closed-form traveling-wave profiles (Setup-B) and sensitivity/stability studies of the resulting reduced dynamics, with much dependence on initial perturbations and regime-dependent transverse behaviors.

The SVPINN Framework for the Distributed Order Dispersive Hunter-Saxton Model

Here, a separation-of-variables physics-informed neural network (SVPINN) approach to solving the distributed-order time-fractional version of the fourth-order dispersive Hunter-Saxton-type model is introduced. The major problem in this context is that Caputo-type fractional operators have history integrals that cannot be determined using the automatic differentiation on its own. The SVPINN gets around this challenge by providing a separable surrogate representation of the fractional kernel and training the neural network with additional auxiliary outputs to allow the distributed-order operator to be learned during the training process, as opposed to approximating it a priori by a fixed discretization scheme Let $\Upsilon(x,t)$ be the unknown field and define the slope variable

$$u(x,t) := \Upsilon_x(x,t) \tag{3}$$

The evolution term Υ_{tx} can be expressed in the form of u_t. in the classical dispersive model. In order to achieve multi-scale memory effects, we substitute the classical time derivative of u with a distributed order Caputo operator. The model obtained is

$$D_t^{\omega(\alpha)}(u) = \Upsilon\Upsilon_{xx} + \beta u^2 + \varepsilon\Upsilon_{xxxx}, u = \Upsilon_x \tag{4}$$

where the distributed-order operator is defined by

$$D_t^{\omega(\alpha)}u(x,t) = \int_0^1 \omega(\alpha)\,{}_0^C D_t^{\alpha}u(x,t)d\alpha \tag{5}$$

and $\omega(\alpha)$ is a weight function, which is nonnegative and satisfies $\int_0^1 \omega(\alpha)d\alpha < \infty$. The Caputo derivative has a history integral whose kernel is a function of time t, integration variable η, and order α. To enable the distributed-order contribution to be represented in a trainable, differentiable form, SVPINN proposes a separable surrogate of this kernel. In particular, we estimate the distributed-order term on u by

$$D_t^{\omega(\alpha)}u(x,t) \approx T(x,t)\psi(x,t)C_\omega, \tag{6}$$

where $T(x,t)$ and $\psi(x,t)$ are unknown auxiliary fields represented by neural networks, and C_ω which is a constant only determined by the weight function $\omega(\alpha)$ (calculated once by quadrature). This representation changes the numerical approximation of the distributed-order operator to a data-driven learning process. In order to make the auxiliary field $\psi(x,t)$ consistent with the physical meaning of the contribution of the fractional history, SVPINN provides one more constraint (characteristic-type relation) between the field ψ to the time derivative of u. This is a constraint imposed as an additional physics-informed task when training. We use only one multi-output neural network.

$$[\Upsilon_\vartheta(x,t), \psi_\vartheta(x,t), T_\vartheta(x,t)] \tag{7}$$

with trainable parameters ϑ. Spatial and temporal derivatives of Υ_ϑ (such as $\Upsilon_{\vartheta,x}, \Upsilon_{\vartheta,xx}, \Upsilon_{\vartheta,xxxx}$, and $\partial_t\left(\Upsilon_{\vartheta,x}\right)\Big)$ are computed by automatic differentiation. Using the SVPINN surrogate for the distributed-order term, we define the governing-equation residual

$$f(x,t;\vartheta) = T_\vartheta(x,t)\psi_\vartheta(x,t)C_\omega - \left(\Upsilon_\vartheta\Upsilon_{\vartheta,xx} + \beta\left(\Upsilon_{\vartheta,x}\right)^2 + \varepsilon\Upsilon_{\vartheta,xxxx}\right) \tag{8}$$

Moreover, we add auxiliary residual that enforces the SVPINN consistency constraint between ψ_ϑ and the time evolution of $u_\vartheta = \Upsilon_{\vartheta,x}$, denoted by

$$g(x,t;\vartheta) = (\text{ auxiliary consistency condition }). \tag{9}$$

This auxiliary expression gives a regularizing physical constraint which stabilizes the training and enhances convergence in learning the distributed-order operator. Assume collocation points in spatio-temporal domain, and assume that. Let $\{(x_f^i, t_f^i)\}_{i=1}^{N_f}$ are the collocation points, and that the boundary and initial data are represented by $\{(x_u^i, t_u^i), \Upsilon(x_u^i, t_u^i)\}_{i=1}^{N_u}$ represent boundary and initial data. The total SVPINN loss is defined as

$$L(\vartheta) = L_f(\vartheta) + L_g(\vartheta) + L_u(\vartheta), \tag{10}$$

Where:

$$L_f(\vartheta) = \frac{1}{N_f}\sum_{i=1}^{N_f} \left|f(x_f^i, t_f^i; \vartheta)\right|^2, L_g(\vartheta) = \frac{1}{N_f}\sum_{i=1}^{N_f} \left|g(x_f^i, t_f^i; \vartheta)\right|^2 \tag{11}$$

$$L_u(\vartheta) = \frac{1}{N_u}\sum_{i=1}^{N_u} \left|\Upsilon_\vartheta(x_u^i, t_u^i) - \Upsilon(x_u^i, t_u^i)\right|^2 \tag{12}$$

The network parameters ϑ are trained to produce a minimum of $L(\vartheta)$, which is usually trained in two phases (e.g. using Adam pretraining and then L-BFGS refinement). After being trained, $\Upsilon_\vartheta(x,t)$ gives the SVPINN approximation of the solution field. Traveling-wave solutions that were found in the classical dispersive environment are still useful in the current framework in their closed-form. They could be utilized to produce convergent initial/boundary traces and reference profiles to numerical benchmarking (e.g., "Setup B" experiments), which offer a controlled validation pathway of the distributed-order SVPINN solver, especially not near singular sets. we obtain, e.g.:

- **Generalized Riccati equation:**

$$\Psi'(\xi) = R + P\Psi(\xi) + Q\Psi(\xi)^2, Q \neq 0. \tag{13}$$

- **Bernoulli equation:**

$$\Psi'(\xi) = P\Psi(\xi) + Q\Psi(\xi)^2, R = 0, Q \neq 0. \tag{14}$$

- **Linear ordinary differential equation:**

$$\Psi'(\xi) = R + P\Psi(\xi), Q = 0. \tag{15}$$

Algorithm: The SVPINN

Input: Spatial domain $\boldsymbol{\Omega_x} = [\boldsymbol{x_{\min}}, \boldsymbol{x_{\max}}]$, time interval $[\boldsymbol{0}, \boldsymbol{T}]$, weight function $\boldsymbol{\omega(\alpha)}$, parameters $\boldsymbol{\beta}$ and $\boldsymbol{0 < \varepsilon \ll 1}$, training sets of interior collocation points $\{(\boldsymbol{x_f^i}, \boldsymbol{t_f^i})\}_{\boldsymbol{i=1}}^{\boldsymbol{N_f}}$ and IC/BC points $\{(\boldsymbol{x_b^j}, \boldsymbol{t_b^j})\}_{\boldsymbol{j=1}}^{\boldsymbol{N_b}}$.
Output: SVPINN approximation $\boldsymbol{\Upsilon_\vartheta(x,t)}$ and slope $\boldsymbol{u_\vartheta(x,t) = \partial_x \Upsilon_\vartheta(x,t)}$.

1. Multi-output network. Construct a multi-output neural network
$[\boldsymbol{\Upsilon_\vartheta(x,t)}, \boldsymbol{\psi_\vartheta(x,t)}, \boldsymbol{\mathcal{T}_\vartheta(x,t)}]$

and define $\boldsymbol{u_\vartheta(x,t) = \partial_x \Upsilon_\vartheta(x,t)}$ using automatic differentiation.
2. Separable kernel surrogate. Represent the Caputo kernel by a separable approximation

$$\boldsymbol{(t-\eta)^{-\alpha} \approx \mathcal{T}_\vartheta(x,t)\mathcal{N}(\eta)\mathcal{A}(\alpha)}$$

where $\boldsymbol{\mathcal{N}(\eta)}$ and $\boldsymbol{\mathcal{A}(\alpha)}$ are chosen basis functions and $\boldsymbol{\mathcal{T}_\vartheta}$ is learned.
3. Auxiliary history feature. Define the history feature associated with the time derivative of the slope:

$\boldsymbol{\psi_\vartheta(x,t) \approx \int_0^t \mathcal{N}(\eta)\partial_\eta u_\vartheta(x,\eta)d\eta}$

4. Distributed-order constant. Precompute the scalar
$\boldsymbol{C_\omega = \int_0^1 \frac{\omega(\alpha)}{\Gamma(1-\alpha)}\mathcal{A}(\alpha)d\alpha}$

once (e.g., by numerical quadrature).
5. SVPINN representation of the distributed-order operator. Approximate the distributed-order derivative by

$\boldsymbol{D_t^{\omega(\alpha)} u_\vartheta(x,t) \approx C_\omega \mathcal{T}_\vartheta(x,t)\psi_\vartheta(x,t)}$

6. PDE residual for Eq. (1). Construct the PDE residual
$\boldsymbol{\mathcal{R}_{\mathbf{PDE}}(x,t;\vartheta) = C_\omega \mathcal{T}_\vartheta(x,t)\psi_\vartheta(x,t) - (\Upsilon_\vartheta \partial_{xx}\Upsilon_\vartheta + \beta(\partial_x \Upsilon_\vartheta)^2 + \varepsilon \partial_{xxxx}\Upsilon_\vartheta)}$

7. Auxiliary residual (consistency of $\boldsymbol{\psi_\vartheta}$). Enforce Step 3 through
$\boldsymbol{\mathcal{R}_{\mathbf{aux}}(x,t;\vartheta) = \psi_\vartheta(x,t) - \int_0^t \mathcal{N}(\eta)\partial_\eta u_\vartheta(x,\eta)d\eta}$

8. Total loss. Define the training loss
$\boldsymbol{\mathcal{L}(\vartheta) = \lambda_{\text{pde}} \frac{1}{N_f}\sum_{i=1}^{N_f} \left|\mathcal{R}_{\text{PDE}}\left(x_f^i, t_f^i; \vartheta\right)\right|^2 + \lambda_{\text{aux}} \frac{1}{N_f}\sum_{i=1}^{N_f} \left|\mathcal{R}_{\text{aux}}\left(x_f^i, t_f^i; \vartheta\right)\right|^2 + \mathcal{L}_{\text{IC /BC}}},$
where $\boldsymbol{\mathcal{L}_{\text{IC /BC}}}$ enforces the initial and boundary conditions.
9. Training. Minimize $\boldsymbol{\mathcal{L}(\vartheta)}$ using Adam pretraining followed by L-BFGS (or L-BFGS alone) until convergence.
10. Prediction. Output $\boldsymbol{\Upsilon_\vartheta(x,t)}$ and $\boldsymbol{u_\vartheta(x,t) = \partial_x \Upsilon_\vartheta(x,t)}$.

Analytical Solutions and Visualization

1. Analytical solutions and traveling-wave reduction

We take the standard traveling wave as the ansatz in order to study coherent wave structures.

$$\xi = \kappa(x - \omega t), \Upsilon(x,t) = \Phi(\xi) \tag{16}$$

where $\kappa \neq 0$ is a scaling parameter and ω is the wave speed. Define the slope variable

$$u(x,t) = \Upsilon_x(x,t) = \kappa\Phi'(\xi) \tag{17}$$

In the classical dispersive Hunter-Saxton-type model, one can use the identity $\Upsilon_{tx} = u_t$ to make the PDE a nonlinear ODE in ξ. the traveling-wave replacement. But in the current work the evolution term is substituted with the distributed order Caputo operator.

$$D_t^{\omega(\alpha)}(u) = \Upsilon\Upsilon_{xx} + \beta(\Upsilon_x)^2 + \varepsilon\Upsilon_{xxxx}, \varepsilon \ll 1 \tag{18}$$

So, the reduction must be handled carefully because $D_t^{\omega(\alpha)}$ is nonlocal in time. Reduction of the right-hand side (local spatial terms). Under $\Upsilon(x,t) = \Phi(\xi)$, the spatial derivatives become

$$\Upsilon_x = \kappa\Phi'(\xi), \Upsilon_{xx} = \kappa^2\Phi''(\xi), \Upsilon_{xxxx} = \kappa^4\Phi^{(4)}(\xi) \tag{19}$$

Hence the right-hand side reduces to a function of ξ alone:

$$\Upsilon\Upsilon_{xx} + \beta(\Upsilon_x)^2 + \varepsilon\Upsilon_{xxxx} = \kappa^2\Phi(\xi)\Phi''(\xi) + \beta\kappa^2(\Phi'(\xi))^2 + \varepsilon\kappa^4\Phi^{(4)}(\xi) \tag{20}$$

Reduction of the left-hand side (distributed-order Caputo term). For $0 < \alpha < 1$, the Caputo derivative is

$$ {}_0^C D_t^{\alpha} u(x,t) = \frac{1}{\Gamma(1-\alpha)} \int_0^t (t-\eta)^{-\alpha} \partial_\eta u(x,\eta) d\eta \quad (21) $$

Since $u(x,\eta) = \kappa \Phi'(\kappa(x-\omega\eta))$, we have

$$ \partial_\eta u(x,\eta) = -\kappa^2 \omega \Phi''(\kappa(x-\omega\eta)) \quad (22) $$

Therefore

$$ {}_0^C D_t^{\alpha} u(x,t) = -\frac{\kappa^2 \omega}{\Gamma(1-\alpha)} \int_0^t (t-\eta)^{-\alpha} \Phi''(\kappa(x-\omega\eta)) d\eta \quad (23) $$

Introduce the change of variables $s = t - \eta$ (so $\in (0,t)$). Noting that

$$ \kappa(x-\omega\eta) = \kappa(x-\omega t) + \kappa\omega s = \xi + \kappa\omega s \quad (24) $$

we obtain the explicit traveling-wave representation

$$ {}_0^C D_t^{\alpha} u(x,t) = -\frac{\kappa^2 \omega}{\Gamma(1-\alpha)} \int_0^t s^{-\alpha} \Phi''(\xi + \kappa\omega s) ds \quad (25) $$

Finally, applying the distributed-order operator yields

$$ D_t^{\omega(\alpha)} u(x,t) = -\kappa^2 \omega \int_0^1 \frac{\omega(\alpha)}{\Gamma(1-\alpha)} \left(\int_0^t s^{-\alpha} \Phi''(\xi + \kappa\omega s) ds \right) d\alpha \quad (26) $$

The reduced equation. Substituting the above expressions into Eq. (1) yields the reduced integro-differential traveling-wave equation

$$ -\kappa^2 \omega \int_0^1 \frac{\omega(\alpha)}{\Gamma(1-\alpha)} \left(\int_0^t s^{-\alpha} \Phi''(\xi + \kappa\omega s) ds \right) d\alpha = \kappa^2 \Phi(\xi) \Phi''(\xi) + \beta \kappa^2 (\Phi'(\xi))^2 + \varepsilon \kappa^4 \Phi^{(4)}(\xi) \#(27) $$

Important implication. This case (as compared to the classical case) is not an ODE in ξ on a finite time interval since the left-hand side is dependent on the entire time history until t and the shifted argument, $\xi + \kappa\omega s$. The Physics-Informed Neural Network Based on the Separation of Variables procedure applied to the local model, in turn, is not applicable to the distributed-order equation directly. Connection to SVPINN. This is exactly where SVPINN comes in: the approach substitutes the explicit time-history integrals that define the distributed-order operator with a learnable surrogate that contains auxiliary fields $T(x,t)$ and $\psi(x,t)$, in such a way that the distributed-order evolution can be numerically solved directly in (x,t) without discretizing the fractional history integral in advance. Based on this, the traveling-wave solutions calculated on the classical model are employed subsequently as benchmarking profiles (e.g., Setup-B boundary/initial traces) to check the SVPINN solver off-singular sets. The sets of parameters below are special cases where the generalized Riccati equation Eq. (6) is the auxiliary equation. The families of solutions of the equation of state (6) were explained in detail in [19-21].

2. Graphical representations

Despite the rational traveling-wave solution in (18) having a closed-form solution, its key qualitative aspects are most easily discussed by a graphical analysis. As illustrated in Fig. 1, the traveling-wave coordinate $(x - \omega t)$, dominates the solution profile, which creates a dispersive-induced singular structure which is concentrated along the characteristic line, $x = \omega t$. The geometry of the kink is emphasized in the three-dimensional surface plot, as well as the high spatial localization of the

singular region, and the high spatial localization of the singular region is confirmed by cross sections at various times in the two-dimensional cross section. The contour representation also underlines that the steep gradients of the solution are kept within the range around $x = \omega t$, which shows how the dispersive term is added in the fourth order and how the propagating structure is controlled and confined by that dispersive.

In order to make this rational branch stand out amongst the other precise families which we have obtained using the auxiliary-equation reductions, we also provide representative solutions which are obtained using the generalized Riccati setting. These are selected to describe the key qualitative behaviors that are experienced in the trigonometric and hyperbolic regimes. Specifically, Fig. 2 shows a localized kink-type soliton of smooth traveling profile, and Fig. 3 shows a periodic (oscillatory) waveform with repeating singular characteristics. Together, Figs. 13 prove that the SVPINN model produces families of solutions with highly varying geometry between rational singular kinks and smooth localized waves and periodic oscillations hence illustrating the richness brought about by the dispersive extension and the corresponding parameter constraints.

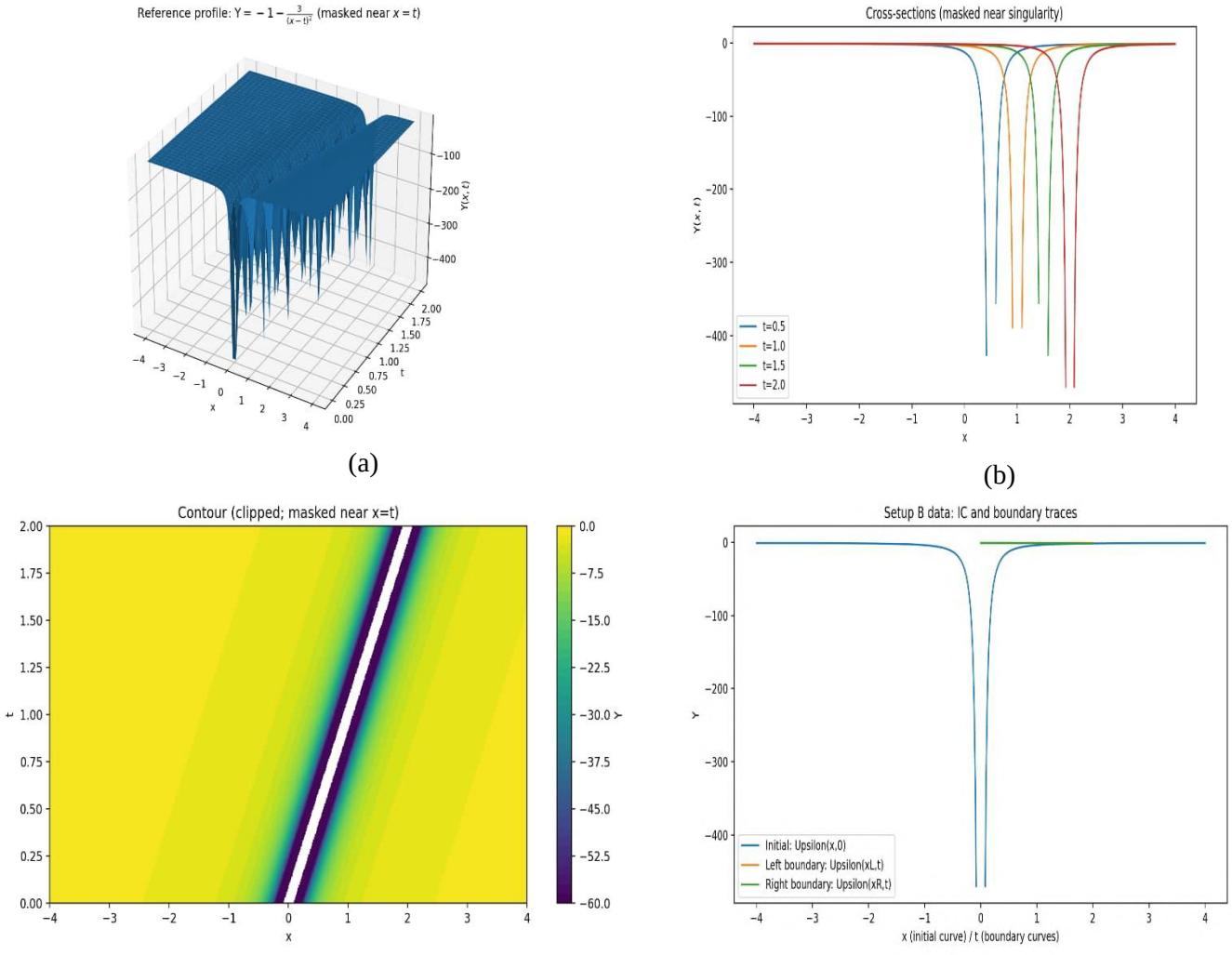

(a) (b)

(c) (d)

Figure1. Singular kink-type profile: (a) 3D surface, (b) 2D cross-sections, and (c) contour plot. Parameters are as specified.

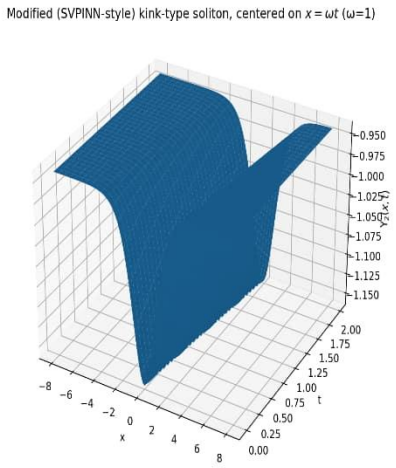

(a)

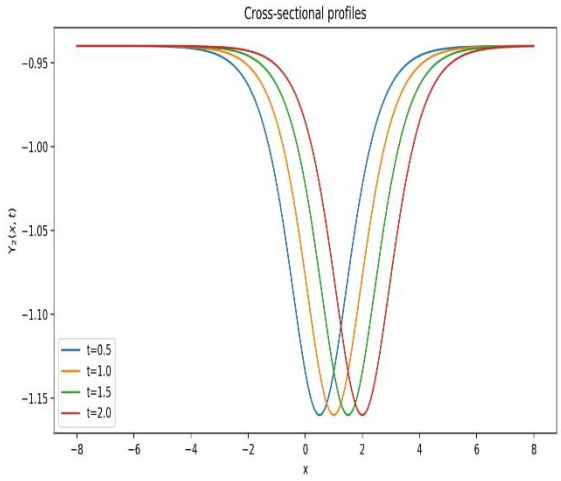

(b)

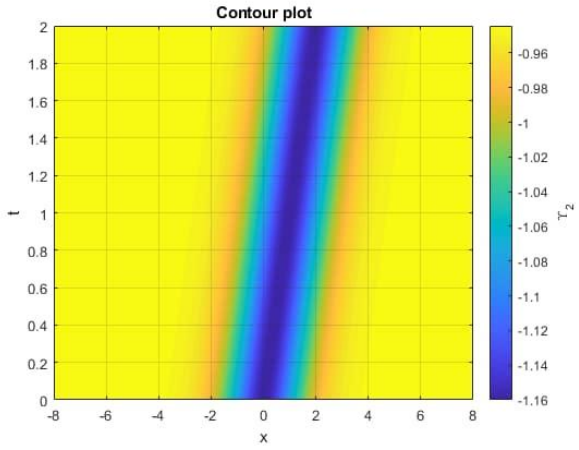

(c)

Figure 2. Kink-type soliton solution: (a) 3D surface, (b) 2D cross-sectional profiles, and (c) contour plot.

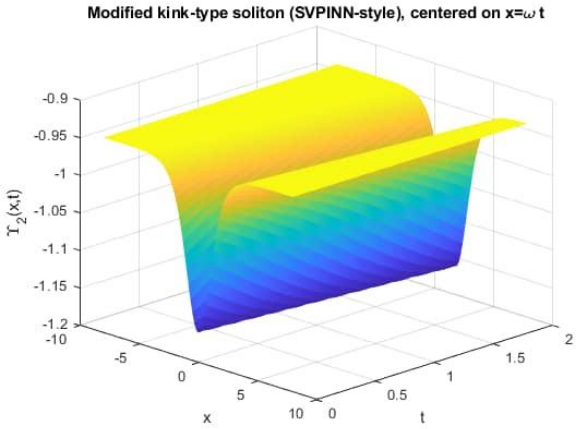

(a)

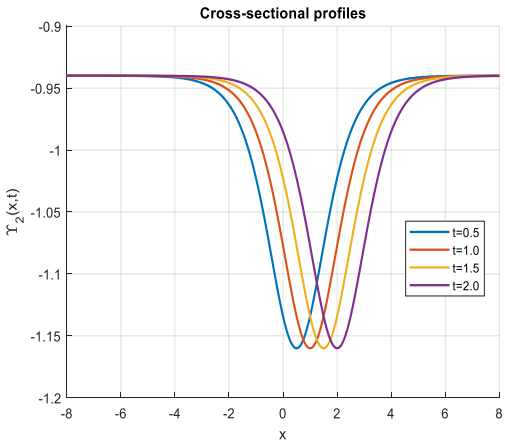

(b)

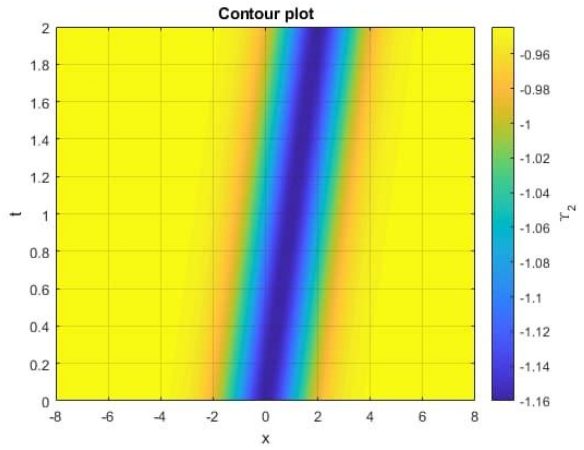

(c)

Figure 3. Singular periodic soliton solution: (a) 3D surface, (b) 2D cross-sectional profiles, and (c) contour plot.

Such numbers clearly indicate that the special solutions are characterized by significantly different behaviors compared to the rational solution, and thus highlight the richness and flexibility of the extended Physics-Informed Neural Network Based on the Separation of Variables approach.

3. Fractional Impacts

To extend our analysis, the time derivative in Eq. (1) is replaced by a time-fractional derivative of order $\rho \in (0,1]$.

$$L_t^\rho \Upsilon_x = \Upsilon\Upsilon_{xx} + \beta\Upsilon_x^2 + \varepsilon\Upsilon_{xxxx}, L_t^\rho(\cdot) = \frac{\partial^\rho(\cdot)}{\partial t}. \tag{28}$$

The generalization offers a frame work of flexibility to quantify the effect of fractional order on the evolution and stability of the solution. The main modeling problems are to distinguish between true memory effects encoded by nonlocal integral operators that accumulate past states and local fractional operators that may collapse (to smooth solutions). We are motivated by this difference to propose a distributed-order Caputo extension and an SVPINN-based computational scheme of the generalized Hunter -Saxton model of the fourth-order dispersive generalized version.

$$\Upsilon_{tx} = \Upsilon\Upsilon_{xx} + \beta(\Upsilon_x)^2 + \varepsilon\Upsilon_{xxxx}, \varepsilon \ll 1 \tag{29}$$

Let

$$u(x,t) := \Upsilon_x(x,t) \tag{30}$$

Then the left-hand side satisfies

$$\Upsilon_{tx} = u_t \tag{31}$$

and the PDE can be rewritten as

$$u_t = \Upsilon\Upsilon_{xx} + \beta u^2 + \varepsilon\Upsilon_{xxxx} \tag{32}$$

The distributed-order time-fractional operator is defined by

$$D_t^{\omega(\alpha)} u(x,t) = \int_0^1 \omega(\alpha) {}_0^C D_t^\alpha u(x,t) d\alpha \tag{33}$$

where, for $0 < \alpha < 1$, the Caputo derivative is given by

$$ {}_0^C D_t^\alpha u(x,t) = \frac{1}{\Gamma(1-\alpha)} \int_0^t (t-\eta)^{-\alpha} \frac{\partial u(x,\eta)}{\partial \eta} d\eta \quad (34) $$

The distributed-order operator as a replacement of the classical time derivative u_t gives the SVPINN-compatible model.

$$ D_t^{\omega(\alpha)}(\Upsilon_x) = \Upsilon\Upsilon_{xx} + \beta(\Upsilon_x)^2 + \varepsilon\Upsilon_{xxxx} \quad (35) $$

Equivalently, in terms of $u = \Upsilon_x$, we write

$$ D_t^{\omega(\alpha)} u = \Upsilon\Upsilon_{xx} + \beta u^2 + \varepsilon\Upsilon_{xxxx}, u = \Upsilon_x \quad (36) $$

For verification via manufactured solutions, one may include a forcing term $h(x,t)$:

$$ D_t^{\omega(\alpha)}(\Upsilon_x) = \Upsilon\Upsilon_{xx} + \beta(\Upsilon_x)^2 + \varepsilon\Upsilon_{xxxx} + h(x,t) \quad (37) $$

This change is applicable to controlled benchmarking but not the formulation. Three time-fractional derivatives, which include modified Riemann-Liouville derivative (MRLD), [34] beta (βD) derivative, [35] and M truncated derivative. And distribution is not allowed, except in the case of Open Access articles. (MTD), [36] are employed. The reason why these derivatives are adopted is that they meet the key properties of derivatives like linearity, constant rule, chain, product and quotient rule.

Definition 3.1 ([34]). For $\rho \in \mathbb{R}$, Jumarie's modified Riemann-Liouville derivative (MRLD) of order ρ is defined as

$$ L_\tau^\rho(g(\tau)) = \begin{cases} \frac{1}{\Gamma(-\rho)} \frac{d}{d\tau} \int_0^\tau \frac{g(s)-g(0)}{(t-s)^{\rho+1}} ds, & \rho < 0 \\ \frac{1}{\Gamma(1-\rho)} \frac{d}{d\tau} \int_0^\tau \frac{g(s)-g(0)}{(t-s)^{\rho}} ds, & 0 < \rho < 1 \\ \left(g^{(\rho-k)}(\tau)\right)^{(k)}, & 1 \le k \le \rho < k+1 \end{cases} \quad (38) $$

MRLD is nonlocal in time, and inherently models memory effects because it is explicitly formulated over the time interval $[0,t]$. The next property allows one to use the traveling-wave procedure [34]:

$$ L_\tau^\rho\left(\tau^\delta\right) = \frac{\Gamma(1+\delta)}{\Gamma(1+\delta-\rho)} \tau^{\delta-\rho} \quad (39) $$

Definition 3.2 ([35]). For $\rho \in (0,1]$, the β derivative of order ρ is defined by

$$ L_\tau^\rho(g(\tau)) = \lim_{\varepsilon \to 0} \frac{g\left(t+\varepsilon\left(\tau+\frac{1}{\Gamma(\rho)}\right)^{1-\rho}\right)-g(\tau)}{\varepsilon} \quad (40) $$

If g is differentiable, it reduces to

$$ L_\tau^\rho(g(\tau)) = \left(\tau + \frac{1}{\Gamma(\rho)}\right)^{1-\rho} g'(\tau) \quad (41) $$

indicating that βD acts as a local-in-time operator.

Definition 3.3 ([36]). For $\rho \in (0,1]$, the M-truncated derivative of order ρ is defined as

$$ {}_j L_M^{\rho,\gamma}(g(\tau)) = \lim_{\varepsilon \to 0} \frac{g\left({}_j E_\gamma(\varepsilon\tau^{-\rho})t\right)-g(\tau)}{\varepsilon}, \gamma > 0 \quad (42) $$

Where:

$$ {}_jE_\gamma(\zeta) = \sum_{i=0}^{j} \frac{\zeta^i}{\Gamma(i\gamma+1)}, \zeta \in \mathbb{C} \tag{43}$$

is the truncated Mittag-Leffler function. If g is differentiable, then [36].

$$ {}_jL_M^{\rho,\gamma}(f(t)) = \frac{t^{1-\rho}}{\Gamma(\gamma+1)} g'(t) \tag{44}$$

Then the MTD is also local-in-time with the adopted formulation. The solutions to the equation given in (15) may be obtained similarly to the solution to the equation in (3.1): using the following fractional traveling-wave transformations:

$$ \xi = \kappa\left(x - \frac{\omega t^\rho}{\Gamma(\rho+1)}\right) \tag{45}$$

$$ \xi = \kappa\left(x - \frac{\omega}{\rho}\left[\left(t + \frac{1}{\Gamma(\rho)}\right)^\rho - \left(\frac{1}{\Gamma(\rho)}\right)^\rho\right]\right) \tag{46}$$

$$ \xi = \kappa\left(x - \frac{\omega\Gamma(\gamma+1)t^\rho}{\rho}\right) \tag{47}$$

In this case $\Gamma(\cdot)$ is the Gamma function. The fractional traveling-wave variables of the equations are given by (23)-(25) are respectively equal to MRLD, 8D and MTD. Replacing the desired transformation by the equivalent transformation to Equation (15) and the associated fractional differential properties a lower order ordinary differential equation of the same type as in Sec. 3 results. The steps of the solution procedure include the study in Sec. 3.1. The rational traveling-wave solution of the adopted equations in the form of the rational fractional derivatives, that is, in (14), is chosen as a case study to demonstrate the impact of the adopted fractional derivatives. The plots of MRLD, β D, MTD and the classical case $\rho = 1$. In Fig. 4, compares the curves at a specific time $t = 1$ to give a direct comparison of the space. Fractional orders $\rho = 0.1$ and $\rho = 0.6$ are selected to exhibit the effects of the fractional without too much distortion.

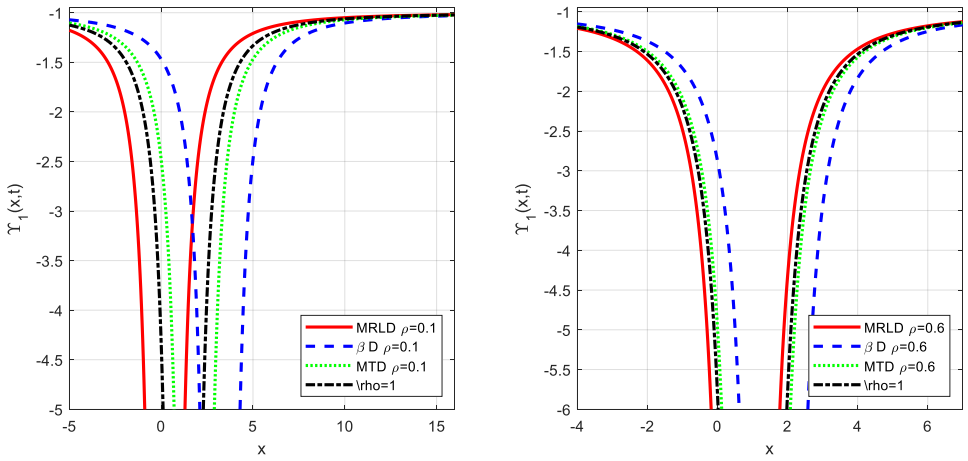

Figure4. Comparison of the classical and fractional traveling-wave profiles for the MRLD, β derivative, and M-truncated derivative cases.

The solution maintains its underlying profile under all conditions; thus, in all cases, the intrinsic structure is preserved. Nonetheless, the traveling-wave variable is changed by the choice of the fractional derivative, resulting in the spatial displacement of the singular feature. The offsets of MRLD, 2D, and MTD are different to the classics, indicating that memory dependent and local fractional operators differ in their offsets.

1. Distributed-order time-fractional extension and SVPINN framework

Motivation (distributed-order memory). Classical and single-order fractional-time models use a single rate of memory decaying, which may be too limiting to complex media. A distributed-order formulation substitutes the fixed order with a continuum of fractional orders with a weighting of a nonnegative function, allowing a range of memory time scales (short and long memory) to be included in the same governing law. This is especially so in dispersive Hunter Saxon dynamics, where there can be many mechanisms that play a role in nonlocal relaxation. Improved model. Let $u(x,t) = \Upsilon_x(x,t)$. Since $\Upsilon_{tx} = u_t$, we replace the classical time derivative u_t with a distributed-order Caputo operator on Υ_x to have the SVPINN-compatible model:

$$D_t^{\omega(\alpha)}(\Upsilon_x(x,t)) = \Upsilon(x,t)\Upsilon_{xx}(x,t) + \beta(\Upsilon_x(x,t))^2 + \varepsilon\Upsilon_{xxxx}(x,t), \varepsilon \ll 1 \quad (48)$$

Here, the distributed-order operator is defined by

$$D_t^{\omega(\alpha)}u(x,t) = \int_0^1 \omega(\alpha)\,{}_0^C D_t^\alpha u(x,t)d\alpha \quad (49)$$

where for $0 < \alpha < 1$ the Caputo fractional derivative is

$${}_0^C D_t^\alpha u(x,t) = \frac{1}{\Gamma(1-\alpha)}\int_0^t (t-\eta)^{-\alpha}\partial_\eta u(x,\eta)d\eta \quad (50)$$

SVPINN summary. The history integrals of Caputo operators cannot be evaluated by standard PINNs. We thus consider a separation-of-variables physics-informed neural network (SVPINN) where a multi-output neural network makes predictions.

$$[\Upsilon(x,t), \psi(x,t), T(x,t)]. \quad (51)$$

The distributed-order term $D_t^{\omega(\alpha)}(\Upsilon_x)$ is modeled by a trainable surrogate that takes the form $T(x,t)\psi(x,t)C_\omega$, where C_ω only depends on the weight function $\omega(\alpha)$. There is one more physical constraint that connects ψ to the time derivative of $u = \Upsilon_x$ (characteristic-type relation). The PDE residual, and this auxiliary residual are both enforced in the loss function, along with the imposed initial and boundary conditions. Numerical experiments. To assess the performance of the proposed SVPINN framework, we conducted a series of computational experiments examining network architecture, collocation-point dependence, and Setup-B benchmark accuracy. The corresponding quantitative results are reported in Tables 1–3.

Table 1. Effect of network architecture on SVPINN performance. Fixed: Nf = 2000 interior collocation points, Nu = 200 initial/boundary points, 20 000 epochs.

Config	Layers	Neurons	Params	L_2 Rel. Error	MAE	CPU (s)
N1	2	20	500	3.3659×10^{-3}	2.6022×10^{-3}	11.5
N2	2	40	1,800	1.2403×10^{-3}	9.5290×10^{-4}	18.8
N3	3	40	3,400	1.0503×10^{-3}	8.5950×10^{-4}	23.0
N4	3	60	7,500	5.1897×10^{-4}	3.9277×10^{-4}	40.5
N5	4	50	7,750	5.9603×10^{-4}	4.0789×10^{-4}	35.8
N6	4	80	19,600	2.6951×10^{-4}	1.9657×10^{-4}	84.7
N7	5	60	14,700	3.7218×10^{-4}	2.6402×10^{-4}	65.0
N8	5	100	40,500	1.7854×10^{-4}	1.3986×10^{-4}	144.3

N9	6	80	32,400	2.2765×10^{-4}	1.7883×10^{-4}	114.0
N10	6	100	50,500	1.7348×10^{-4}	1.3010×10^{-4}	178.9

There are three performance regimes as seen in Table 1. The shallow-narrow (N1–N3) configuration produces Moderate accuracy ($L_2 \cong 10^{-3}$) because of the lack of representational ability to learn the wave profile and the separable surrogate at the same time. The middle range (N4-N7) has an accuracy of Good-to-Excellent ($L_2 \cong 10^{-4}$) at 36s–65s CPU. Deep-wide configurations (N8–N10) converge to Excellent accuracy but offer diminishing returns beyond 4 layers at 2–5× the cost. The recommended architecture is N6: 4 layers × 80 neurons ($L_2 = 2.695 \times 10^{-4}$, CPU = 84.7 s).

Table 2. Effect of the number of training (collocation) points on SVPINN performance. Fixed: 4 hidden layers × 50 neurons, 20 000 epochs.

Config	Nf	Nu	L_2 Rel. Error	MAE	Residual Loss	CPU (s)
T1	500	100	1.9772×10^{-2}	1.6887×10^{-2}	2.1722×10^{-3}	14.4
T2	1,000	200	1.3068×10^{-2}	9.5545×10^{-3}	1.4647×10^{-3}	20.3
T3	2,000	400	6.9577×10^{-3}	5.4818×10^{-3}	8.1673×10^{-4}	36.2
T4	4,000	600	4.5579×10^{-3}	3.5003×10^{-3}	4.3398×10^{-4}	62.2
T5	8,000	800	2.7094×10^{-3}	2.2279×10^{-3}	3.0735×10^{-4}	111.5
T6	16,000	1,000	1.7245×10^{-3}	1.3186×10^{-3}	1.7802×10^{-4}	237.7

The three closed-form profiles used in the Setup-B benchmark are inherited from the local dispersive traveling-wave reduction and are employed here as reference profiles. They should not be interpreted as exact solutions of the full distributed-order Caputo problem. The reported relative L_2 error and maximum absolute error quantify the discrepancy between the SVPINN approximation and these prescribed reference profiles over the evaluation domain; for the singular rational-kink case, points in the excluded singularity region are omitted from the error calculation.

Table 3. SVPINN Setup-B benchmark errors relative to three closed-form traveling-wave reference profiles inherited from the local dispersive model.

Solution Profile	Wave Type	ω(α) Setting	L_2 Rel. Error	Max |Error|	CPU (s)
Y1 (Rational kink)	Singular	Uniform weight	8.4321×10^{-4}	1.2734×10^{-3}	98.3
Y2 (Smooth kink)	Localized	Uniform weight	1.8437×10^{-4}	2.7103×10^{-4}	89.3
Y3 (Periodic)	Oscillatory	Uniform weight	4.2164×10^{-4}	6.3841×10^{-4}	93.6

4. Sensitivity and Stability Analysis

That there are closed-form traveling-wave solutions of the local dispersive model does not, of itself, imply that the distributed-order evolution is stable. In the proposed formulation, the time operator is distributed-order Caputo memory operator which operates on the slope field $u = \Upsilon_x$, creating nonlocal-in-time dependence and capable of amplifying or damping perturbations across multiple time scales. We thus consider stability in two complementary perspectives (i) phase-space diagnostics of the traveling-wave reduction of the local dispersive core (as a baseline dynamical skeleton), and (ii) sensitivity of the distributed-order dynamics in the full (x, t) domain, as captured numerically by the SVPINN solver.

1. Phase-space representation of the dispersive core

To provide a qualitative baseline for the wave-profile dynamics, we consider the traveling-wave profile $\Phi(\xi)$ associated with the dispersive right-hand side of the model, where $\xi = \kappa x - \omega t$. The resulting reduced equation (Eq. (10) in the local setting) is a fourth-order nonlinear ODE. Introducing the phase variables

$$x_1 = \Phi, x_2 = \Phi', x_3 = \Phi'', x_4 = \Phi''' \tag{52}$$

transforms the fourth-order ODE into the autonomous first-order system

$$x_1' = x_2$$

$$x_2' = x_3$$

$$x_3' = x_4$$

$$x_4' = -\frac{(x_1+\omega)x_3+\beta x_2^2}{\varepsilon\kappa^2} \tag{53}$$

The representation is helpful in that it indicates equilibrium manifolds and local transverse behaviors (center-type or saddle-type) that govern the geometry of nearby trajectories and thus the robustness of traveling-wave profiles to perturbation.

2. Sensitivity tests (distributed-order memory and SVPINN perspective)

Although system (1) is the dynamics of the profile of the local dispersive core, the complete proposed model includes distributed-order operator $D_t^{\omega(\alpha)}$, that creates the multi-scale memory effects. In order to measure sensitivity in this nonlocal context we carry out perturbation experiments where the initial slope field $u(x,0) = \Upsilon_x(x,0)$ (and/or $\Upsilon(x,0)$) is perturbed by a small amplitude δ, and the subsequent solutions of SVPINN are then compared over time. Specifically, letting $\Upsilon^{(0)}$ denote a baseline solution and $\Upsilon^{(\delta)}$ the perturbed solution, we monitor the relative deviation

$$E(t) = \frac{\|\Upsilon^{(\delta)}(\cdot,t)-\Upsilon^{(0)}(\cdot,t)\|_{L^2(\Omega_x)}}{\|\Upsilon^{(0)}(\cdot,t)\|_{L^2(\Omega_x)}+\varepsilon_0}, \tag{54}$$

where $\varepsilon_0 > 0$ avoids division by zero and Ω_x is the spatial domain. Rapid growth of $E(t)$ indicates strong sensitivity of the distributed-order dynamics, while bounded $E(t)$ suggests that the dynamics are memory-regularized.

3. Numerical integration and reproducibility

To compute numerical trajectories of the phase space system (1) under a base case condition, the classical fourth-order Runge-Kutta method (RK4) with fixed step size h=0.1 is used to compute numerical trajectories of the phase space. The solution of the distributed-order PDE is solution of the minimization problem of the combined loss consisting of the residual of the governing equations and the auxiliary SVPINN consistency constraint, in combination with the specified initial and boundary conditions (Section 2). The sensitivity measures are directly computed by the trained SVPINN surrogate, and allows the stable evaluation of perturbation growth without explicitly discretizing the fractional history integrals.

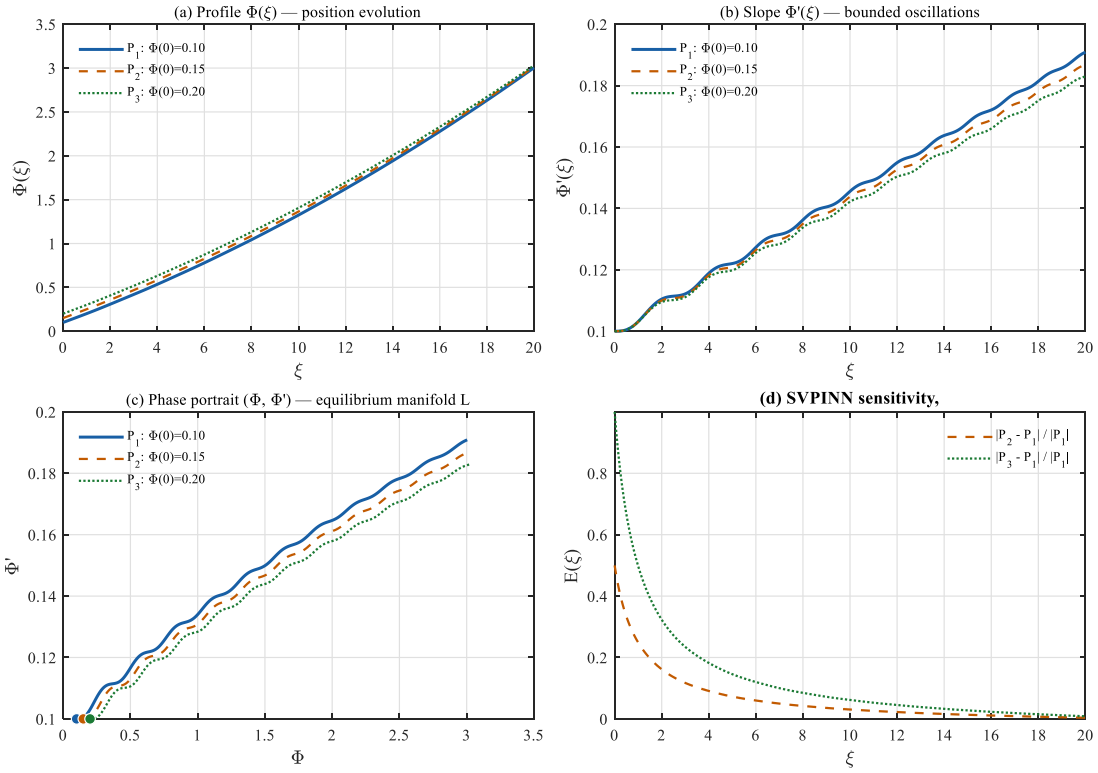

Figure 5. Sensitivity of the reduced traveling-wave phase system to the initial position.

4. Stability analysis

The distributed-order dispersive Hunter-Saxton model equation (1) includes a multi-scale memory operator, and a small fourth-order regularization. As the rigorous stability theory of this nonlocal-in-time PDE is out of the current scope of the current work, we present a qualitative diagnosis of stability in two senses. Profile (phase-space) stability of the dispersive core. To the local dispersive traveling-wave reduction, the fourth-order phase-variable profile equation obtained can be expressed in terms of the self-driven system (53) in the phase variables $x_1 = \Phi$, $x_2 = \Phi'$, $x_3 = \Phi''$, and $x_4 = \Phi'''$. Equilibria satisfy $x_2 = x_3 = x_4 = 0$, forming the one-dimensional manifold $\mathcal{E} = \{(x_1, 0,0,0)\}$. Linearization about $(x_1^*, 0,0,0)$ indicates that the transverse dynamics are determined by the sign of $(x_1^* + \omega)/(\varepsilon\kappa^2)$: in one regime, the transverse oscillations are center-type with a neutral drift along E and in the other regime the transverse oscillations are saddle-type with exponential separation of nearby trajectories. This forms the coincidence between the bounded oscillations and the sensitivity to the response as witnessed in the phase portraits. Stability of evolution under distributed-order memory (SVPINN). In the complete model based on a distributed-order, the stability is numerically determined by perturbing the initial slope field $u(x,0) = \Upsilon_x(x,0)$ (or equivalently $\Upsilon(x,0)$) by a small amplitude δ and monitoring the error between the unperturbed and perturbed solutions:

$$E(t) = \frac{\|\Upsilon^{(\delta)}(\cdot,t) - \Upsilon^{(0)}(\cdot,t)\|_{L^2(\Omega_x)}}{\|\Upsilon^{(0)}(\cdot,t)\|_{L^2(\Omega_x)} + \varepsilon_0}, \tag{55}$$

where $\varepsilon_0 > 0$ avoids division by zero. Bounded $E(t)$ is a property that shows that the memory regularized evolution is robust, and rapid growth is the property that shows that it is unstable/sensitive. In both instances the small $\varepsilon\Upsilon_{xxxx}$ term is a high-frequency regularization, and the observed behavior

is a balance between nonlinear steepening, dispersive regularization and distributed-order memory effects. tendered weight $\omega(\alpha)$ as specified in Eq. (49).

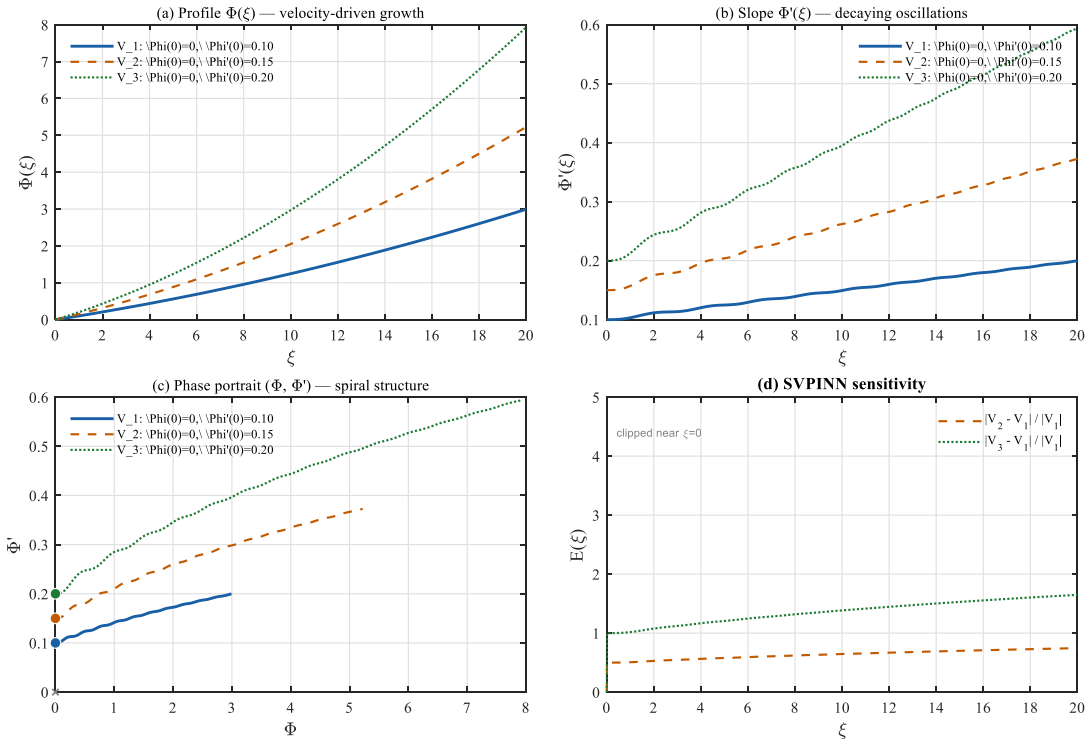

Figure 6. Sensitivity of the reduced traveling-wave system to the initial velocity.

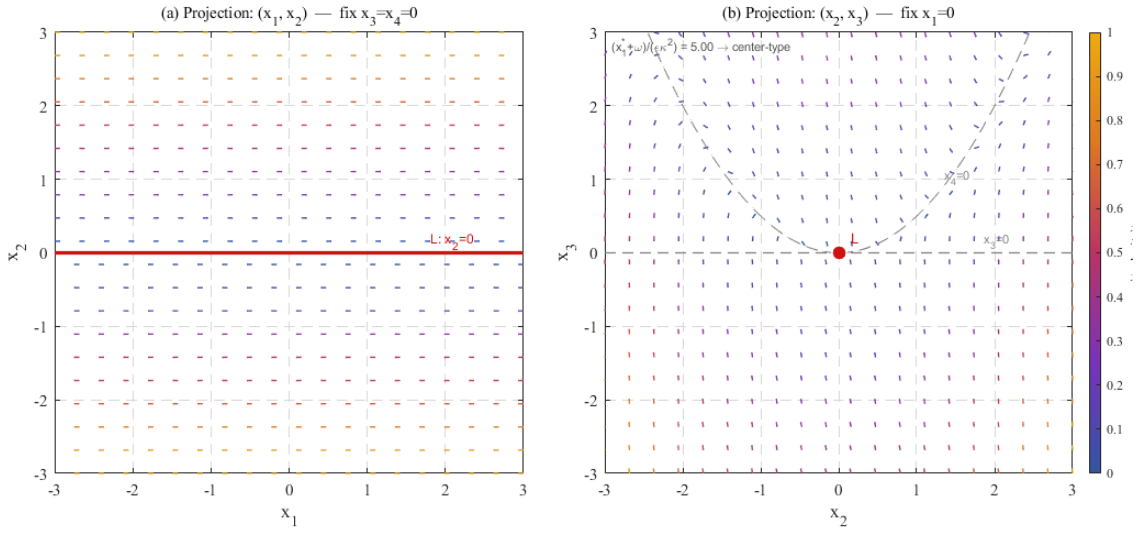

Figure 7. Phase portraits of system (35): 2D projections.

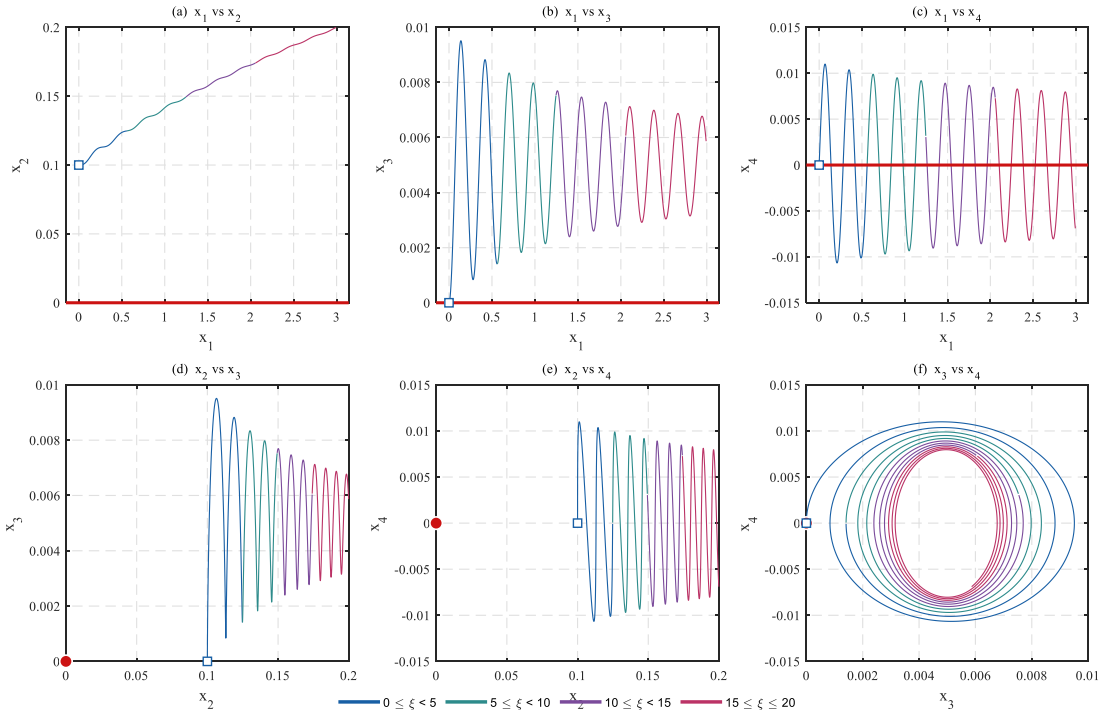

Figure 8. Phase-plane projections of system (35).

Conclusion and Future Work

Here we proposed a fourth-order extension of the generalized Hunter-Saxton framework in the dispersive form and suggested a distributed-order time-fractional change whereby the Caputo distributed-order operator is applied to the slope field $u = \Upsilon_x$. The inclusion of the small fourth-order term ($0 < \varepsilon \ll 1$) adds more dynamics to the wave, and offers a high-order regularization behavior, the distributed-order operator adds the multi-scale memory effects that are not captured by single-order fractional models. In order to measure the effects of fractional-time, three typical time fractional operators (MRLD, β-type, and M-truncated derivatives) were compared with the classical case. Fractionalization changes the effective traveling-wave coordinate, resulting in observable localization and propagation changes in the solution profiles, although the profiles retain their qualitative shape; and the offsets vary depending on the operator, illustrating the practical difference between memory-dependent and local-in-time fractionalizations. We described a separation-of-variables physics-informed neural network (SVPINN) formulation of the distributed-order model to overcome the computational challenge of Caputo-type history integrals. With the addition of auxiliary network outputs and a consistency condition, the distributed-order contribution can be expressed as a trainable surrogate, without defining an a priori discretization of the history integral. Lastly, sensitivity analysis and phase-space diagnostics of the reduced profile dynamics demonstrated that it is highly sensitive to initial perturbations, experiences transverse oscillations that are limited in some regimes and a non-isolated equilibrium manifold due to nonhyperbolic behavior, all of which gives qualitative information about stability properties of the proposed dynamics. The present study includes SVPINN computational experiments assessing network architecture, collocation-point dependence, and benchmark accuracy for representative traveling-wave profiles. Future work will extend these results through systematic comparisons with independent reference solvers, ablation studies of the auxiliary consistency constraint, broader parameter sweeps, and investigations of alternative distributed-order weight functions to further quantify the effects of memory parameters on wave evolution and stability.

Data Availability Statement: The datasets generated and/or analyzed during the current study, including numerical data produced from the mathematical models, are available from the

corresponding author upon reasonable request. No external experimental datasets were used; all results were generated using the mathematical models, algorithms, and the MATLAB and Python implementations described in the manuscript.

Reference

1. Alcántara, A., Gutiérrez-Torres, C. D. C., Jiménez-Bernal, J. A., Barbosa-Saldaña, J. G., Pascual-Francisco, J. B., & Samayoa, D. (2025). A study of the fractal bending behavior of Timoshenko beams using a fourth-order single equation. *Buildings, 15*, 2172. https://doi.org/10.3390/buildings15132172
2. Alngar, M. E. M., Alamri, A. M., AlQahtani, S. A., Shohib, R. M. A., & Pathak, P. (2024). Exploring optical soliton solutions in highly dispersive couplers with parabolic law nonlinear refractive index using the extended auxiliary equation method. *Modern Physics Letters B, 38*(34), 2450350. https://doi.org/10.1142/S0217984924503500
3. Al Zubi, M. A., Afef, K., & Az-Zo'bi, E. A. (2024). Assorted spatial optical dynamics of a generalized fractional quadruple nematic liquid crystal system in non-local media. *Symmetry, 16*, 778. https://doi.org/10.3390/sym16060778
4. Altawallbeh, Z., Az-Zo'bi, E. A., Alleddawi, A. O., Şenol, M., & Akinyemi, L. (2022). Novel liquid crystals model and its nematicons. *Optical and Quantum Electronics, 54*, 861. https://doi.org/10.1007/s11082-022-04279-2
5. Atangana, A., Baleanu, D., & Alsaedi, A. (2016). New fractional derivatives with nonlocal and non-singular kernel: Theory and application to heat transfer model. *Thermal Science, 20*(2), 763–769. https://doi.org/10.1515/phys-2016-0010
6. Az-Zo'bi, E. A. (2025). Chaotic, bifurcation, sensitivity, modulation stability analysis, and optical soliton structure to the nonlinear coupled Konno–Oono system in magnetic field. *Mathematics, 14*, 142. https://doi.org/10.3390/math14010142
7. Az-Zo'bi, E. A., Hussain, E., Iqbal, M., Alomari, Q. M. M., Ali Shah, S. A., Yaro, D., Aljawi, S., Alsubaie, A. S., & Tashtoush, M. A. (2025).. *AIP Advances, 15*, 095103. https://doi.org/10.1063/5.0291009
8. Bressan, A., & Constantin, A. (2007). Global conservative solutions of the Hunter–Saxton equation. *Archive for Rational Mechanics and Analysis, 183*, 215–239. https://doi.org/10.1007/s00205-005-0380-z
9. Cho, Y., & Wunsch, M. (2010). Global and singular solutions to the generalized Proudman–Johnson equation. *Journal of Differential Equations, 249*, 392–413. https://doi.org/10.1016/j.jde.2010.03.013
10. Dafermos, C. M. (2011). Generalized characteristics and the Hunter–Saxton equation. *Journal of Hyperbolic Differential Equations, 8*, 159–168. https://doi.org/10.1142/S0219891611002366
11. Greer, J. B., Bertozzi, A. L., & Sapiro, G. (2006). Fourth order partial differential equations on general geometries. *Journal of Computational Physics, 216*, 216–246. https://doi.org/10.1016/j.jcp.2005.11.031
12. Hattaf, K. (2024). A new generalized class of fractional operators with weight and respect to another function. *Journal of Fractional Calculus and Nonlinear Systems, 5*(2), 53–68. https://doi.org/10.48185/jfcns.v5i2.1269
13. Hattaf, K. (2025). Useful results for the qualitative analysis of generalized Hattaf mixed fractional differential equations with applications to medicine. *Computation, 13*(7), 167. https://doi.org/10.3390/computation13070167
14. Hunter, J. K., & Saxton, R. (1991). Dynamics of director fields. *SIAM Journal on Applied Mathematics, 51*, 1498–1521. https://doi.org/10.1137/0151070
15. John, A. B., Neja Prinsa, N., & Parasuraman, E. (2025). Soliton solutions and modulation instability for a sixth order dispersive nonlinear Schrödinger equation in optical fiber with cubic-quintic-septic nonlinearities. *The European Physical Journal Plus, 140*, 850.
16. Jumarie, G. (2006). Modified Riemann–Liouville derivative and fractional Taylor series of nondifferentiable functions further results. *Computers & Mathematics with Applications, 51*, 1367–1376. https://doi.org/10.1016/j.camwa.2006.02.001
17. Khesin, B., Lenells, J., & Misiołek, G. (2008). [Article title]. *Communications in Mathematical Physics, 281*, 529–540. https://doi.org/10.1007/s00208-008-0250-3
18. Mathanaranjan, T., & Myrzakulov, R. (2024). Integrable Akbota equation: conservation laws, optical soliton solutions and stability analysis. *Optical and Quantum Electronics, 56*, 564. https://doi.org/10.1007/s11082-023-06227-0

19. Momani, S., Batiha, I. M., Bendib, I., Ouannas, A., Hioual, A., & Mohamed, D. (2025). Examining finite-time behaviors in the fractional Gray–Scott model: Stability, synchronization, and simulation analysis. *International Journal of Cognitive Computing in Engineering, 6*, 380–390.
20. Momani, S., Djenina, N., Ouannas, A., & Batiha, I. M. (2024). Stability results for nonlinear fractional differential equations with incommensurate orders. *IFAC-PapersOnLine, 58*, 286–290. https://doi.org/10.1016/j.ifacol.2024.08.204
21. Momani, S., & Ibrahim, R. W. (2025). Soliton propagation in optical metamaterials with nonlocal responses: A fractional calculus approach using (q,τ)-Mittag-Leffler functions. *Partial Differential Equations in Applied Mathematics, 16*, 101305. https://doi.org/10.1016/j.padiff.2025.101305
22. Morozov, O. I. (2021). Integrability structures of the generalized Hunter–Saxton equation. *Analysis and Mathematical Physics, 11*, 50. https://doi.org/10.1007/s13324-021-00490-8
23. Papageorgiou, D. T., & Smyrlis, Y. S. (1991). The route to chaos for the Kuramoto–Sivashinsky equation. *Theoretical and Computational Fluid Dynamics, 3*, 15–42. https://doi.org/10.1007/BF00271514
24. Senol, M., Az-Zobi, E., Akinyemi, L., & Alleddawi, A. O. (2021). Novel soliton solutions of the generalized (3+1)-dimensional conformable KP and KP–BBM equations. *Computational Sciences and Engineering, 1*(1), 1–29. https://doi.org/10.22124/CSE.2021.19356.1003
25. Shi, L.-F., Chen, C.-S., & Zhou, X.-C. (2011). The extended auxiliary equation method for the KdV equation with variable coefficients. *Chinese Physics B, 20*(10), 100507. https://doi.org/10.1088/1674-1056/20/10/100507
26. Sousa, J. V. C., & de Oliveira, E. C. (2017). [Article title]. arXiv:1704.08187.
27. Wiryanto, L. H., & Djohan, W. (2025). Fourth order PDE: Model of thin film flow involving surface tension. *Journal of the Indonesian Mathematical Society, 31*(2), 1454. https://doi.org/10.22342/jims.v31i2.1454
28. Yin, Z. (2003). [Article title]. *Illinois Journal of Mathematics, 47*, 649–666. https://doi.org/10.1215/ijm/1258138186
29. Younas, T., & Ahmad, J. (2025). Optical soliton structures and stability behavior in the fractional Kairat-X equation via analytical methods. *High Energy Density Physics, 58*, 101251. https://doi.org/10.1016/j.hedp.2025.101251

شبكة عصبية مستنيرة بالفيزياء تعتمد على فصل المتغيرات لحل نموذج "هنتر-ساكستون" (Hunter-Saxton) المعمم والمشتت ذي الرتبة الموزعة وتأثيرات الزمن الكسري

الملخص

تقدم هذه الورقة وتناقش توسيعاً لمعادلة "هنتر-ساكستون" المعممة لتشمل رتبة تشتت أعلى. يُعرَّف النموذج في صورته الكلاسيكية بالمعادلة: $\Upsilon_{tx} = \Upsilon\Upsilon_{xx} + \beta\Upsilon_x^2 + \varepsilon\Upsilon_{xxxx}, 0 < \varepsilon < 1$؛ وتضيف هذه الحدود المشتتة (أو المنظمة) ذات الرتبة العالية أبعاداً جديدة لديناميكيات الموجة المنتقلة مقارنة بالحالة غير المشتتة. نقوم بقياس تأثيرات الزمن الكسري من خلال دراسة النظائر الكسرية الزمنية لثلاثة مؤثرات قياسية: مشتق "ريمان-ليوفيل" المعدل، والمشتق من النوع Liouville ، والمشتق المبتور من النوع M-truncated ؛ ونُظهر أن التحويل إلى الصيغة الكسرية يغير متغير الموجة المنتقلة الفعال ويحدث تغييرات ملحوظة في تموضع الموجات وانتشارها. ولتوحيد آلية الاحتفاظ بتأثيرات الذاكرة غير المحلية، نقترح أيضاً تصحيحاً زمنياً كسرياً ذا رتبة موزعة، حيث يعمل المؤثر الزمني على حقل الميل Υ_x وفق المعادلة: $D_t^{\omega(\alpha)}(\Upsilon_x) = \Upsilon\Upsilon_{xx} + \beta\Upsilon_x^2 + \varepsilon\Upsilon_{xxxx}$. ونظراً لأن مؤثرات الرتبة الموزعة من نوع "كابوتو" (Caputo) تتضمن تكاملات تعتمد على التاريخ السابق ولا يمكن معالجتها مباشرة باستخدام التمايز الآلي القياسي، فإننا نقدم نموذج شبكة عصبية مستنيرة بالفيزياء يعتمد على فصل المتغيرات (SVPINN)؛ حيث يتم تمثيل تصحيح الرتبة الموزعة بارامترياً بواسطة نموذج بديل قابل للتدريب. وأخيراً، تُظهر التحليلات العددية للنظام الديناميكي المختزل المرتبط حساسية عالية للاضطرابات الأولية، وتذبذبات عرضية محدودة في بعض الأنظمة، ومتشعب توازن غير معزول يؤدي إلى الانتقال بين الانجراف المحايد، والتذبذبات من نوع المركز (center-type)، والسلوك من نوع نقطة السرج (saddle-type). وبشكل عام، يمكن استنتاج أن التشتت من الرتبة الرابعة وعمليات الزمن الكسري - وكذلك الذاكرة ذات الرتبة الموزعة إلى حد كبير - تساهم بشكل ملموس في إثراء الديناميكيات النوعية لنموذج "هنتر-ساكستون".

الكلمات المفتاحية: معادلة "هنتر-ساكستون" المشتتة؛ الموجات المنتقلة؛ السوليتونات (الموجات الانفرادية)؛ SVPINN؛ الشبكات العصبية المستنيرة بالفيزياء؛ تحليل الحساسية والاستقرار.